Computational Modelling of Concrete and Concrete Structures – Meschke, Pichler & Rots (Eds)

Autogenous healing in cement: A kinetic Monte Carlo simulation of $CaCO_3$ precipitation

Aleena Alex
Newcastle University, UK

Enrico Masoero
Cardiff University, UK

ABSTRACT: Autogenous healing induced by the dissolution of C-S-H and CH in a cracked cement paste was modelled in this study, at the mesoscale of tens of nanometres. The pore solution contains carbon dioxide (CO_2) resulting in the precipitation of calcium carbonate ($CaCO_3$) into the crack. The simulations were performed using MASKE, a recently developed coarse-grained Kinetic Monte Carlo framework where the molecules of the solid phases are modelled as mechanically interacting particles that can also precipitate and dissolve. The precipitation of $CaCO_3$ molecules was initially observed in tiny gel pores within the C-S-H, but eventually extends completely filling the crack. The mechanical properties of the healed system were also investigated by straining the simulation box, computing the corresponding virial stress, and plotting the resulting stress-strain relationship.

1 INTRODUCTION

1.1 *Self-healing in concrete*

Concrete from Ordinary Portland Cement (OPC) is quasi-brittle construction material which can withstand high compressive load. During its life cycle, microcracks can develop within its structure. Microcracks are too small (<0.1 mm) to significantly affect the mechanical strength of a structure, but they do make the cement matrix more permeable. This increases the likelihood of chemical attack and corrosion of reinforcement, which may ultimately compromise the structural integrity of concrete (Qureshi et al. 2018). Self-healing is a possible solution to this issue.

Self-healing is classified as (1) Autogenous healing: where the materials in concrete continue to react with water in the cement paste forming new hydration product that seal the cracks, or (2) Autonomous healing: where sealing agents (such as bacteria) are encapsulated in the cement matrix and become active when a crack changes its local exposure conditions.

1.2 *Autogenous healing models*

Autogenous healing in cement/concrete can occur in 2 ways: (1) Continuous hydration at the crack where previously anhydrous cement comes in contact with water/moisture. The anhydrous cement reacts with water producing hydration products, such as calcium silicate hydrate (C-S-H) and calcium hydroxide (CH); Another way is (2) the dissolution of C-S-H, CH and other hydration products that have already formed in the cement matrix, releasing ions that react with dissolved carbon dioxide (CO_2) in the pore solution. This process eventually precipitates carbonates that fill the cracks (mainly calcium carbonate, $CaCO_3$, although other alkali ions, such as Na or K, may contribute with other carbonates too, especially in low-calcium cements).

Very few models exist which describe autogenous healing. Some models were proposed to predict the amount of unhydrated cement present in the matrix after hydration based on the water-cement (w/c) ratio and the fineness of cement (He et al. 2007). This is an indirect measure of the self-healing potential of the sample. Traditionally, continuous hydration of residual anhydrous phases was believed to be the governing self-healing mechanism. However, in recent years it has been shown that continued hydration reduces in a few weeks after casting, whereas calcite formation from existing hydration product becomes the main mechanism of healing afterwards (Van Tittelboom & De Belie 2013). Numerical models have been proposed for autogenous healing by both the mechanisms (further hydration and calcite formation). Huang et al. (2013) proposed a reactive transport model for the self-healing of microcracks in cement paste by further hydration. They established the relationship between self-healing efficiency and extra water provided. Hilloulin et al. (2014) reported a combined

DOI 10.1201/9781003316404-12

hydro-chemo-mechanical model to simulate autogenous healing which also predicts the mechanical regain after healing. Chitez and Jefferson (2016) combined the existing approaches to propose a comprehensive mathematical model for early age autogenous healing. The model uses reactive water transport to predict the movement of healing materials (C-S-H and CH) under a thermo-hygro-chemical (THC) framework. This model also predicts early age crack healing due to continuous hydration and is not applicable to long term calcite formation. It was only in recent years that calcite formation induced healing was attempted to be modelled. Ranaivomanana and Benkemoun (2017) proposed a numerical model in which chemical reactions and transport phenomena were modelled for the porous matrix and the crack by diffusion and permeation. .

While hydration induced self-healing has been studied extensively, models on calcite formation induced autogenous self-healing are far and few between. The existing models have their own strength, but also are limited in the mechanistic description of $CaCO_3$ precipitation, and this limits the possibility to use them to explore new solutions. For instance, altering the chemistry of the phases favouring $CaCO_3$ formation as a way to control the rate of the process or even the morphology of the carbonates to optimize healing. This study aims to address calcite induced self-healing and the resulting mechanical regain using a discrete particle-based model.

2 METHODOLOGY

2.1 *Overview*

In this study we have examined autogenous healing by simulating a crack in a paste of C-S-H and CH under the assumption of full hydration. The size of the simulated system is kept very small, with crack with size of 1 nm only. In this way we can use kinetic constants for individual reactions and model these directly from Transition State Theory, without involving additional assumptions to further coarse grain the system (Shvab et al. 2017). Once generated, the crack was filled with water and CO_2 at atmospheric saturation level which was kept constant throughout the simulation. This induces the dissolution of both C-S-H and, most significantly, CH releasing free calcium ions. These ions then react with the CO_2 resulting in the precipitation of $CaCO_3$ and healing the crack.

2.2 *MASKE: A kinetic Monte Carlo framework*

The simulations were performed using MASKE, a recently developed Kinetic Monte Carlo framework (Shvab et al. 2017). In MASKE, the system is discretized representing the mineral phases as agglomerates of nanoparticles which interact via effective potentials (energy as a function of distance) whose spatial derivatives are the interaction forces. The particles can dissolve and precipitate via reaction rates obtained from transition state theory (TST). These rates depend on macroscopic rate constants for the chemical reactions involved, the saturation index of the solution with respect to each reaction and the excess free energy coming from the interactions between particles. This excess free energy is particularly important because it renders the solubility of individual particles dependent on local morphology i.e. the number of interacting neighbours as well as the presence of any local mechanical stress.

The dissolution and precipitation rates for a particle are described by Equations 1 and 2.

$$r_{diss} = \frac{k_B T}{h} V_m \frac{c^*}{\gamma^*} exp\left[-\frac{\Delta G^*}{k_B T}\right] exp\left[\frac{-\Delta U_{diss} - U_{kink}}{k_B T}\right] \quad (1)$$

$$r_{prec} = \frac{k_B T}{h} V_m \frac{c^*}{\gamma^*} exp\left[-\frac{\Delta G^*}{k_B T}\right] \beta_{prec} \quad (2)$$

where kB: Boltzmann constant; T: temperature, K; h: Planck constant; γ^*: activity coefficient; c^*: standard state concentration; V_M: molar volume of the particle; ΔG^*: standard state activation energy for dissolution; β_{prec}: saturation index of the solution. ΔU_{diss} is the change in interaction energy following the dissolution of a particle and ΔU_{kink} is the interaction energy between kink particle and its nearest neighbour. The derivation and physical meaning of these equations and its validation are discussed in detail in earlier works (Coopamootoo & Masoero 2020; Shvab et al. 2017).

2.3 *Simulation steps*

The simulations were carried out in 6 steps:

(1) Starting from an initially empty simulation box, CH crystals were created by agglomerating nanoparticles representing individual CH molecules, until reaching a volume fraction of 28% in the box. This is the theoretical volume fraction of CH in a paste obtained from fully hydrated C_3S if the C-S-H is assumed to have a gel porosity of 34.5% (Masoero et al. 2014).
(2) A spherical agglomerate of randomly closed packed C-S-H particles was created separately and parametrized to get the correct interaction potential parameters for C-S-H. This ensured that the C-S-H grain made of the agglomerated particles is at equilibrium (no dissolution nor precipitation). The equilibrium is reached when the activity product of the surrounding solution coincides with the equilibrium constant of C-S-H (i.e., saturation index ($\beta = 1$)).
(3) Other interaction potentials such as C-S-H/CH, C-S-H/$CaCO_3$ and CH/$CaCO_3$ were analytically determined averaging the interaction strength between pure phases.

(4) Once the interaction potentials were determined, the box was filled to the prescribed volume fraction of solid C-S-H (47%). This leaves 25% gel porosity in the system.
(5) The C-S-H / CH system was then cracked by carving out a 1nm thick slice of particles from the center of the box.
(6) The dissolution-mineralization in and around the crack was finally simulated using MASKE.

These steps are detailed in the sections below.

2.4 *Creating $Ca(OH)_2$ crystals*

This first simulation was to create two crystallites of $Ca(OH)_2$, targeting a desired volume fraction $\eta = 28\%$. This η assumed that the paste was pure C_3S and was fully hydrated, hence leading only to C-S-H gel and $Ca(OH)_2$ as hydration products. The C-S-H gel was assumed to have an internal gel porosity of approximately 34.5%, whereas the $Ca(OH)_2$ was considered be a solid crystal. The volume fractions occupied by the two minerals were then obtained from the stoichiometry and molar volumes (Masoero et al. 2014). It was also assumed that the uncracked paste features no capillary pores.

Two small face centered cubic (FCC) nuclei of $Ca(OH)_2$ were created (Figure 1 (a)) with different orientations, and setting the solution to a high concentration of Ca^{2+} and OH^-, so that further precipitation will occur. Snapshots were saved during the simulation and a configuration with $\eta \approx 28\%$ was chosen (Figure 1(b)).

2.5 *Parameterising amorphous C-S-H for solubility*

The particles in MASKE interact via harmonic potentials as described in Coopamootoo and Masoero (2020).

$$U(r) = \frac{1}{2}k(r - r_0)^2 - \varepsilon_0 \qquad (3)$$

where U is the interaction energy, r is the interparticle distance, $k = EA/r_0$, E being the Young's modulus of the particle and $r_0 = \pi D_0^2/4$ and ε_0 is the minimum energy at equilibrium. $\varepsilon_0 = \gamma\Omega/n_{kink}$, where γ is the surface energy, Ω is the surface area of particle and n_{kink} number of neighbors for a kink particle. A kink particle has half the number of neighbors as a bulk particle. For an FCC packed CH n_{kink} is easily determined. However, for amorphous C-S-H it was estimated by a trial-and-error process.

A random close packing (RCP) of C-S-H particles were created separately in another simulation box. This was done using the random space filling algorithm in Masoero & Di Luzio 2020. The equilibrium distance between interacting C-S-H particles was set to be smaller than the actual molecular diameters, to compensate for the porosity of a random close packing and eventually obtain a dense C-S-H with same density as solid C-S-H without pores. See Coopamootoo 2020 paper for a similar approach, although there aimed at producing non-porous C_3S. Attention was paid to zero the average axial stresses on the dense C-S-H system.

An iterative scheme was employed to compute the number of interacting neighbors in the bulk of the dense C-S-H domain, which in turn defines the interaction potential between C-S-H particles: see Coopamootoo and Masoero (2020) for details on how the number of neighboring particles in the bulk and the water-solid interfacial energy of a phase can be used to obtain interaction parameters. When the RCP with consistent interactions was obtained, a spherical grain was carved out and the surrounding solution was set to match the equilibrium constant for C-S-H dissolution. At this stage, the bond energy of C-S-H was tweaked until the correct zero-rate of dissolution/precipitation was obtained.

2.6 *Parameterising amorphous C-S-H/CH*

The relations described in section 2.5 were used to determine the interaction potentials of particles from the same solid phase. However, for two particles

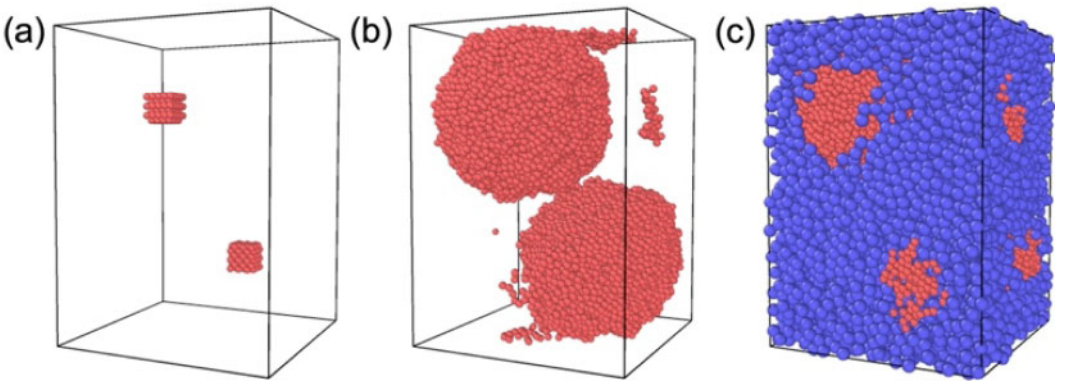

Figure 1. Box size 14x14x10 nm. CH (red) and C-S-H (blue). (a) Two FCC seeds of CH were placed in the box (b) CH precipitation carried out to the desired 28% and (c) C-S-H packed to 47%.

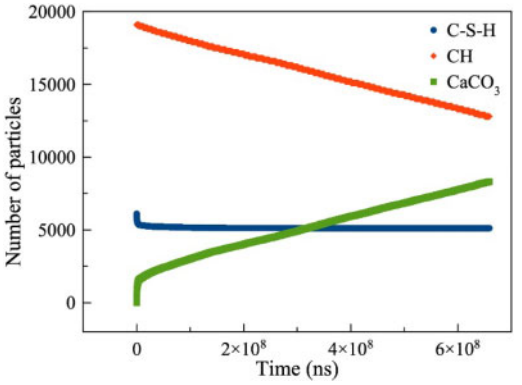

Figure 2. Number of particles vs time as the simulation proceeds. Results are provided for the first 15000 steps.

representing different phases, 1 and 2, such as C-S-H and CH, it was assumed that the minimum interaction energy can be determined by the expression

$$\varepsilon_{12} = \varepsilon_{21} = (k_{12}\gamma_1 + k_{21}\gamma_2)\frac{A_1}{n} \quad (4)$$

where $k_{12} = k_{21}$ was assumed to be on average 0.5. This factor is a measure of individual surface energy contribution towards the interaction potential between surfaces of particles 1 and 2. Detailed atomic scale simulation studies may give a better estimate of k.

2.7 *Packing and relaxing*

Once the interaction potentials between all possible combination of particles were determined, C-S-H was packed to a volume fraction of 47% around the pre-existing CH grains, as presented in Figure 1(c). This leaves 25% of gel pores. This simulation box was then relaxed by energy minimization ensuring that the pressure in all directions was zero. A crack of 1 nm was then created at the centre of the box as shown in Figure 3 (T0).

The concentration of carbonate ions in the implicit solution was fixed to atmospheric saturation levels as determined by Henry's law. Finally, the dissolution-precipitation reactions were run with MASKE and the results were obtained as detailed in the next section.

3 RESULTS AND DISCUSSION

Number of particles of C-S-H, CH and $CaCO_3$ vs time for the first 15000 steps of the simulation is shown in Figure 2. The rates of dissolution of CH and

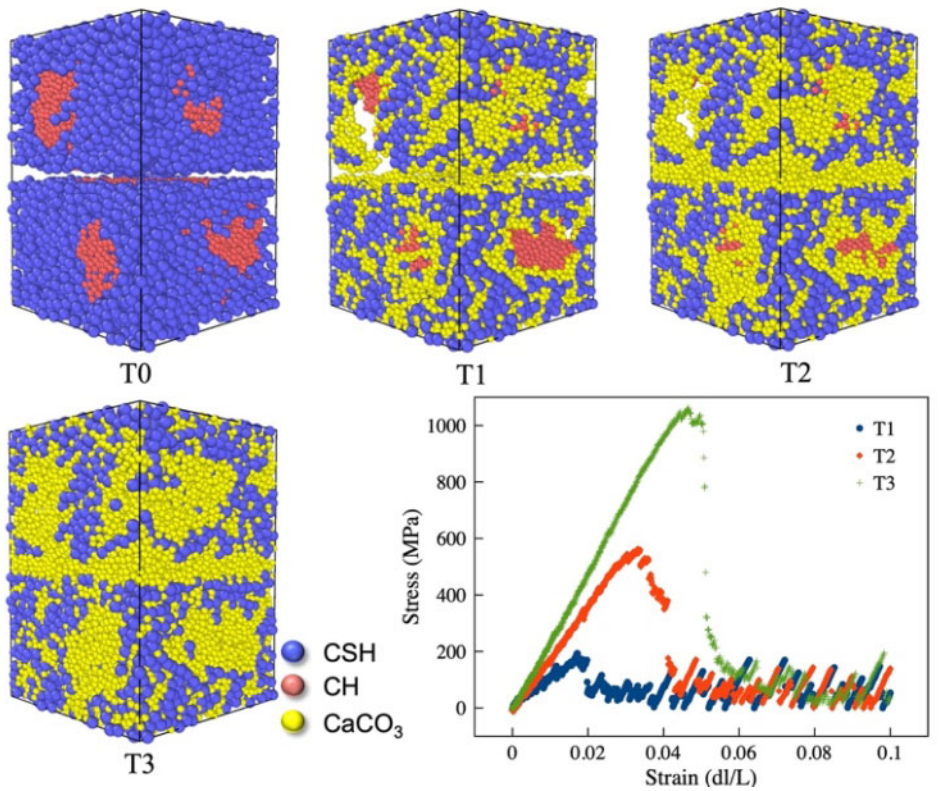

Figure 3. Box size 14x14x10 nm. Crack size 1nm. CH (red) and C-S-H (blue) dissolves precipitating $CaCO_3$ (yellow). Snapshots at 3 consecutive stages (T1, T2, T3) were saved and the evolution of mechanical properties as the crack heals was determined by the stress-strain plot.

precipitation of $CaCO_3$ were found to be constant at this stage. Initially, dissolution of C-S-H particles was observed close to the crack due to the amorphous structure of C-S-H. However, CH dissolution takes over and for the rest of the simulation CH dissolution drives the precipitation of $CaCO_3$. It was observed that initially, the $CaCO_3$ precipitation was predominantly in the gel pores. However, as simulation proceeds precipitation was observed in the crack as well.

3.1 *Mechanical properties*

The crack was entirely bridged by $CaCO_3$ when CH had completely dissolved. The volume occupied by solid particles in the box (with fixed box sizes) increased by 15-20% due to the larger size of $CaCO_3$ compared to CH.

When the crack started to heal (T1 in Figure 3), a snapshot was saved and the box was strained perpendicular to the crack. Stress in the direction of load was determined as the negative of pressure, this latter obtained from the virial method implementation in LAMMPS (Thompson et al. 2022). Stress-strain relationship was plotted as shown in Figure 3. There was a slight regain of mechanical strength ($\sim$100 MPa) at this point. Consequently, on further bridging this regain increases steadily up to $\sim$1000 MPa of ultimate strength (T3 in Figure 2) once the crack was fully bridged.

These strength values are clearly much greater than the tensile strength of cement paste, but one must consider that these simulations are at the nanoscale, hence fracture-inducing defects are very small (consider the scaling of strength with defect size e.g. from Griffith's law). Such high tensile strengths are indeed typically obtained from simulations at the nanoscale on cement hydrates (Lolli et al. 2018).

These simulations show that MASKE is a powerful tool to model the calcite precipitation induced autogenous healing in cementitious systems. Further investigations need to be done on how the chemistry of the solution evolves during the dissolution and precipitation process. Furthermore, all the observations in this work were made at nanoscale. Future research will address the scaling-up to micro and macro scale.

4 CONCLUSIONS

- MASKE was used to simulate dissolution of C-S-H and CH and precipitation of $CaCO_3$ in a model cement paste, leading to autogenous healing.
- A crack of size 1 nm was bridged completely by the precipitated $CaCO_3$. A volume gain of 15–20% was obtained.
- Mechanical properties of the system steadily improved with time.
- A clear strength gain was measured as the crack healed.

ACKNOWLEDGEMENTS

Research funded by the UK Engineering and Physics Research Council, EPSRC, grant EP/S013997/1.

REFERENCES

Chitez, A. S., & Jefferson, A. D. 2016. A coupled thermo-hygro-chemical model for characterising autogenous healing in ordinary cementitious materials. *Cement and Concrete Research 88*: 184–197.

Coopamootoo, K., & Masoero, E. 2020. Simulations of Crystal Dissolution Using Interacting Particles: Prediction of Stress Evolution and Rates at Defects and Application to Tricalcium Silicate. *The Journal of Physical Chemistry C 124*(36): 19603–19615.

He, H., Guo, Z., Stroeven, P., Stroeven, M., & Sluys, L. J. 2007. Self-healing capacity of concrete-computer simulation study of unhydrated cement structure. *Image Analysis & Stereology* 26(3): 137–143.

Hilloulin, B., Grondin, F., Matallah, M., & Loukili, A. 2014. Modelling of autogenous healing in ultra high performance concrete. *Cement and Concrete Research 61*: 64–70.

Huang, H., Ye, G., & Damidot, D. 2013. Characterization and quantification of self-healing behaviors of microcracks due to further hydration in cement paste. *Cement and Concrete Research 52*: 71–81.

Lolli, F., Manzano, H., Provis, J. L., Bignozzi, M. C., & Masoero, E. 2018. Atomistic simulations of geopolymer models: the impact of disorder on structure and mechanics. *ACS applied materials & interfaces 10*(26): 22809–22820.

Masoero, E., & Di Luzio, G. 2020. Nanoparticle simulations of logarithmic creep and microprestress relaxation in concrete and other disordered solids. *Cement and Concrete Research* 137: 106181.

Masoero, E., Thomas, J. J., & Jennings, H. M. 2014. A reaction zone hypothesis for the effects of particle size and water-to-cement ratio on the early hydration kinetics of C_3S. *Journal of the American Ceramic Society* 97(3): 967–975.

Qureshi, T., Kanellopoulos, A. & Al-Tabbaa, A. 2018. Autogenous self-healing of cement with expansive minerals-I: Impact in early age crack healing. *Construction and Building Materials* 192: 768–784.

Ranaivomanana, H., & Benkemoun, N. 2017. Numerical modelling of the healing process induced by carbonation of a single crack in concrete structures: Theoretical formulation and Embedded Finite Element Method implementation. *Finite Elements in Analysis and Design 132*: 42–51.

Shvab, I., Brochard, L., Manzano, H., & Masoero, E. 2017. Precipitation mechanisms of mesoporous nanoparticle aggregates: off-lattice, coarse-grained, kinetic simulations. *Crystal Growth & Design* 17(3): 1316–1327.

Thompson, A. P., Aktulga, H. M., Berger, R., Bolintineanu, D. S., Brown, W. M., Crozier, P. S., ... & Plimpton, S. J. 2022. LAMMPS-a flexible simulation tool for particle-based materials modeling at the atomic, meso, and continuum scales. *Computer Physics Communications 271*: 108171.

Van Tittelboom, K., & De Belie, N. 2013. Self-healing in cementitious materials—A review. *Materials* 6(6): 2182–2217.